AIMS Materials Science, 6(3): 363–376.
DOI: 10.3934/matersci.2019.3.363
Received: 16 February 2019
Accepted: 09 May 2019
Published: 17 May 2019

http://www.aimspress.com/journal/Materials

Research article

Thermoplastic magnetic elastomer for fused filament fabrication

Andrew H. Morgenstern, Thomas M. Calascione, Nathan A. Fischer, Thomas J. Lee, John E. Wentz and Brittany B. Nelson-Cheeseman*

Department of Mechanical Engineering, University of St. Thomas, St. Paul, MN 55105, USA

*** Correspondence:** Email: bbnelsonchee@stthomas.edu.

Abstract: Magnetorheological elastomers (MREs) are unique smart materials of high elasticity and magnetic susceptibility. MREs are prominent for the high degree of mechanical deformation or changes in stiffness that can be induced by applying magnetic fields. While most MREs are made with thermoset elastomers, this research focuses on the development and testing of a thermoplastic magnetic elastomer for potential use as fused filament fabrication (FFF) filament. FFF, also known as 3D printing, is an additive manufacturing technique that consists of 1D viscous thermoplastic extrusions that create 2D layers that build up to a 3D part. This method of creating parts produces underlying anisotropies which can be tuned to control the properties of the final part. Our thermoplastic magnetic elastomer was created utilizing solvent casting techniques to disperse isotropic magnetic particulate within a thermoplastic polyurethane matrix. Samples were created spanning two different magnetic particulate types (<150 μm iron (Fe) & 2–4 μm magnetite (Fe_3O_4)) and each with three different particulate loadings (20, 30, 40 wt%). The material was then extruded into FFF filaments with a Filastruder. Mechanical stress vs. strain curves of the extruded filaments were obtained using an MTS tensile tester. Magnetic hysteresis loops were acquired with a vibrating sample magnetometer (VSM). The analogous pure polyurethane filaments were also extruded and tested as a control. Our testing indeed shows that altering the magnetic particulate type and weight percentage impacts both the magnetic and mechanical properties of the overall material. In general, the filament samples with iron particulate had higher diametric consistency and were more compliant than those with magnetite particulate. Additionally, samples with magnetite had higher magnetic susceptibility and coercivity but lower saturation magnetization than those with iron. Lastly, increasing particulate percentage increases both the mechanical stiffness and saturation magnetization of the samples, as expected.

Keywords: thermoplastic elastomer; magnetic elastomer; filament extrusion; mechanical properties; magnetic properties

1. Introduction

Developments in smart composites are highly sought after today due to their superior qualities and potential for advanced applications. For instance, magnetorheological composites with polymer matrixes have shown to have various functional applications such as smart sensors and actuators due to their magnetoelasticity, wearable technology due to their ductility, manufacturability, and weight, and biomedical drug delivery [1–3]. Magnetorheological elastomers (MREs), in particular, demonstrate specific qualities of interest. Whereas highly elastic and magnetic properties are usually mutually exclusive in naturally occurring materials, the development of MREs has opened the possibility to explore new material uses as actuators, dampers, and soft robotics [4–7]. Some applications of MREs utilize their tunable elastic moduli, whereas others focus on the utility in their inherent anisotropic properties [8]. As with all composites, the properties, relative percentage, and structure of the two components can be used to dictate the mechanical and magnetic properties of the final composite [9–13].

In addition to the dramatic influence composites have had on society, additive manufacturing has increased considerably throughout the past few years with the improvement in fused filament fabrication (FFF) modeling. FFF involves an additive principle by laying down material in layers via a continuous filament fed through a heated moving head. Today FFF is utilizing various types of materials including polymers, ceramics, and composites [14]. There is a near saturation in research focusing on the property and structural analysis of basic materials used in by FFF. A good portion of this research is now focusing on utilizing these basic materials in new ways [15,16]. Others focus on specific understandings for industrial and commercial markets [17–19]. Nonetheless, research on composite materials used in FFF has only scratched the surface. FFF can be seen as a "material science chamber" for mixing and matching materials, properties, and architectures [20]. Prototyping and investigating with materials that can be used in FFF has led to the development of many composites with unique properties [21–26].

Of all the composites used in FFF, magnetic elastomers remain relatively unexplored. The precise and directed structures made possible by FFF could lead to magnetic elastomer structures with enhanced performance. Since FFF is an additive manufacturing technique dependent on viscous flow, filament extrusion and printing would need to be accomplished prior to thermosetting or be completed with a thermoplastic matrix. Previous work has been performed on extruding magnetic elastomers but it has used thermosetting materials, which can involve complicated curing steps [27]. Meanwhile, FFF of a thermoplastic MRE would involve a much simpler printing process. In order to realize this, however, an FFF feedstock filament of MRE must first be successfully developed and fully characterized for its structural, magnetic, and mechanical properties.

In this paper, we demonstrate the development and testing of a thermoplastic MRE extruded filament for use in FFF. More specifically this research investigates the effects of isotropic magnetic particulate type and concentration on the mechanical and magnetic properties of the extruded filament used in nonindustrial 3D printing. We found that the filament samples with iron (Fe_3O_4) particulate had higher diametric consistency and was more compliant than those with equivalent

weight percentage of magnetite (Fe_3O_4) particulate. Additionally, samples with Fe_3O_4 had higher magnetic susceptibility and magnetic coercivity but lower saturation magnetization than those with Fe. Lastly, increasing particulate percentage increased the mechanical stiffness, magnetic susceptibility, and saturation magnetization of the samples. These studies show that a variety of high quality extruded magnetic thermoplastic elastomer filaments are easily accessible for pursuing future FFF of magnetic elastomers. We note that this study is the first step in exploring these magnetic elastomer materials in this extruded filament geometry for future 3D printing. As such, this work focuses on the foundational mechanical and magnetic properties of such samples. Future magneto-mechanical and microstructural characterization of the filaments and their printed counterparts will undoubtedly shed further light on the full functionality and promise of these new materials and geometries.

2. Materials and method

2.1. Materials

Filaments and pellets of NinjaFlex (Thermoplastic Polyurethane (TPU)) were obtained from Fenner Drives. For our purposes, the "water" variant (i.e., uncolored) of the NinjaFlex polymer was obtained. According to the manufacturers data, NinjaFlex filament has a melting point of 216 ℃, a glass transition of −35 ℃ and an elongation of 65% and tensile strength of 4 MPa at yield [28]. Fe (<150 μm) and Fe_3O_4 (2–4 μm) particulate were used as magnetic infill. Historically, these are the two most common magnetic materials used in magnetic elastomers, and their soft magnetic nature allows for fast magnetic response upon applied field. While both contain Fe, the ferromagnetic nature of iron leads to a much larger saturation magnetization compared to the ferromagnetic Fe_3O_4 (where two Fe atoms per formula unit are aligned antiparallel and effectively cancel one another out). Nevertheless, the Fe_3O_4 particulate comes in much smaller sizes, is more uniform in shape, and has been approved in biomedical applications by the FDA. Dimethylformamide (DMF) was used as a solvent.

2.2. Solvent casting

Following the work of Lee et al., NinjaFlex pellets were dissolved in DMF with intermittent stirring at a material to solvent ratio of 1:5 [29]. Once material was fully dissolved and in a viscous solution, magnetic particulate (iron (Fe) or magnetite (Fe_3O_4)) at a determined weight percentage (0, 20, 30, 40 wt%) was slowly stirred into the material. As the particulate was added to the solution, continuous stirring fostered uniform dispersion and helped prevent particulate from bunching up and sticking the sides of the container. The mixed solution was then poured into aluminum trays and placed in a dehydrator heated at 75 ℃ to evaporate the solvent. A coating of Teflon non-stick spray was applied to the interior of each tray before solvent was poured. After allowing for all the solvent to evaporate over a period of 48 hours, the material is ready for extrusion.

2.3. Extrusion

Extrusion of filament samples was accomplished using a filament extrusion device purchased from Filastruder (Figure 1). A Filastruder takes raw material through a feed hole at the top of the

piping, pulls it down with an auger, and extrudes FFF filaments. For this research, filaments were extruded through a 2 mm nozzle. Typically, a Filastruder is fed pellets (rough sphere of approximate 1–2.5 mm dimeter) through a hopper.

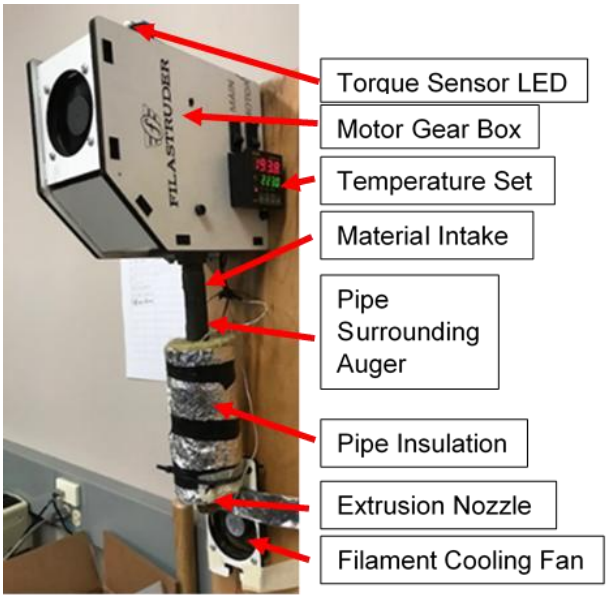

Figure 1. Filastruder used for extrusion of filament.

Extruding the solvent casted material involved its own process. On acquiring the material from the solvent casting procedure, the samples were removed from their molds and cut into pieces approximately 1 cm × 3 cm. These dimensions were determined by measuring the approximate gap formed between the spirals of the auger in the Filastruder and the opening of the feed hole in the piping. The cut pieces were placed back into a dehydrator for storage, to prevent moisture from entering the samples, and to maintain a temperature of approximately 75 ℃. Directly before extrusion, samples were placed in a convection oven and heated to approximately 100 ℃. Having samples at an elevated temperature prior to extrusion helped prevent temperature variance within the Filastruder that could cause jamming or uneven material flow out of the nozzle. Due to the varying melting temperature of the composite materials with different particulate material and weight percentage and preliminary observations, the baseline temperature for initially attempting to extrude was set at 175 ℃.

Once the Filastruder was given appropriate time to maintain a steady temperature, the auger was turned on and material was fed directly into the feed hole. At this temperature none of the material would melt which gave the system adequate time to pull in material to the base of the Filastruder and build up pressure for consistent flow. Once a critical mass of material was fed into the Filastruder, denoted by the flickering of the red LED that marks overloading of the auger motor, the temperature was increased until material flowed out of the nozzle. The quality of the extruded material was monitored, and the temperature was regulated appropriately to find the optimal temperature for extruding material of a visibly consistent diameter with limited flaws. Although the rheological properties of the TPU and composite samples were not measured directly, the filaments were extruded using conditions designed to provide similar viscosities across the range of concentrations.

As torque, output strand quality, and output strand diameter are strongly affected by the viscosity of the extrudate, the extrusion temperature was controlled to allow for consistent strand diameter, strand quality, and torque between samples. All filament sample types studied are summarized in Table 1. The extrusion temperature for each condition is provided in Table 2, and, at each of the temperatures given in Table 2, the viscosity of each material can be considered to be similar to that of each other material. Once the initial material was fully processed through the Filastruder, the filaments were refed into the auger for double extrusion. This process ensured that magnetic particulate was more evenly dispersed in the filament and to achieve more diametric consistency. The filament was then spooled and stored for testing. All the composite filaments were made with the solvent cast elastomer. Upon extrusion, each sample variant was checked for flaws visually and by feeling the filament.

Table 1. Filament sample variants.

No Particulate	Fe Particulate	Fe_3O_4 Particulate
As-purchased TPU filament	20 wt% Fe: 80 wt% TPU	20 wt% Fe_3O_4: 80 wt% TPU
Extruded TPU Pellets	30 wt% Fe: 70 wt% TPU	30 wt% Fe_3O_4: 70 wt% TPU
Extruded Solvent Cast TPU	40 wt% Fe: 60 wt% TPU	40 wt% Fe_3O_4: 60 wt% TPU

2.4. Mechanical measurements

For mechanical testing, a hybrid of ASTM D412 and ASTM D2256 standards was developed for testing the filaments. Testing was accomplished using an MTS Criterion Model 43 tensile testing machine with attached 5 kN Bollard grips, which measured the force vs. displacement curves of the filament material. The strain rate used was 20 in/min (50.8 cm/min), which coincides with the suggested strain rate for pulling elastomer material according to ASTM D412. According to ASDM D2256, the standard for measuring threads and yarns, an unstrained initial length of 10 in (25.4 cm) between grips was desired for testing. To compensate for the remainder of the grip and partial slip, 10 filament samples of 16 in (40.64 cm) were prepared for each material variant. The unstrained initial length was used to compute the strain in the material according to Eq 1.

$$\varepsilon = \frac{\Delta L}{L} \tag{1}$$

where ε is the tensile strain, ΔL is the change in material length, and L is the initial length of material. Samples were each marked and measured at 1-in (2.54 cm) intervals with a caliper for a total of 15 measurements. The interval diameter data was recorded and compared in Microsoft Excel software. The average diameter of each sample was used to compute the average cross-sectional area, which was used to compute the stress in the material according to Eq 2.

$$\sigma = \frac{P}{A} \tag{2}$$

where σ is the tensile stress, P is the applied tensile load, and A is the cross-sectional area.

2.5. Magnetic measurements

A Princeton Applied Research Vibrating Sample Magnetometer (VSM) at the University of Minnesota's Institute for Rock Magnetism was used to measure magnetic hysteresis loops of the samples at room temperature. Three 0.75-in (1.9 cm) samples were randomly prepared from each filament variant. The mass of each sample was taken for determining normalization magnetization. Each sample was then labeled prior to being secured to the vibrating sample holder stick using masking tape. The sample was centered along the three axes between the measurement coils. Hysteresis loops were obtained between +/−1.4 Tesla. Each sample was tested with long axis orientation parallel and perpendicular to the applied magnetic field.

3. Results and discussion

3.1. Sample production

Ten samples of each variant were extruded at varied temperatures because of changing material properties from particulate type and loading. Each variant was extruded at a temperature as dictated by the qualities of the sample. These temperature values are shown in Table 2.

Table 2. Extrusion temperatures of each extruded sample variant.

Material	Extrusion Temp (Celsius)
Pellets	195.0
Solvent Cast	195.0
20 wt% Fe	183.5
30 wt% Fe	184.0
40 wt% Fe	185.0
20 wt% Fe_3O_4	177.0
30 wt% Fe_3O_4	178.0
40 wt% Fe_3O_4	179.0

3.2. Consistency data

The diametric consistency trends can be seen in Table 3. The diametric consistency of the filaments was dependent on multiple factors including extrusion temperature, processing techniques, particulate type and loading. The most consistent samples were extracted at the lower end of the extrusion temperature range for a given material composition. Of the samples with particulate, the Fe samples in general were the most consistent apart from the 40 wt% Fe_3O_4 samples. This is most likely caused by the large amount of aggregation of Fe_3O_4 particles, as discussed by Lee et al. [29]. As observed during extrusion, diametric consistency seemed to be largely dependent on a consistent rate of material being fed into the extruder and the extrusion temperature.

As demonstrated in Table 3, the pooled standard deviation of each sample types' diameters was small enough to produce an acceptable general trend. Determining the exact curve and range of acceptable values due to error propagation and procedural effects are outside the scope of this study.

Table 3. Variability data of tested filament samples.

	As-Purchased	Pellets	Solvent Cast	20 wt% Fe	30 wt% Fe	40 wt% Fe	20 wt% Fe_3O_4	30 wt% Fe_3O_4	40 wt% Fe_3O_4
Avg Diameter (mm)	1.75	1.98	2.01	2.00	1.98	1.93	1.98	1.81	1.85
Pooled Standard Deviation	0	0.0400	0.0622	0.0343	0.0318	0.0276	0.0359	0.0552	0.0270

3.3. Effects of extrusion temperature

In addition to affecting sample consistency, extrusion temperature had a noticeable effect on the mechanical properties of the extruded filament. Figure 2 demonstrates how extrusion temperature and immediate mechanical stiffness are inversely related; as extrusion temperature increases, stiffness decreases. This trend suggests that as the extrusion temperature increases, the disorder and amorphous structure of the polymer within the filament increases, because more amorphous polymers have decreased tensile modulus [30]. The final ordered structure within the polymer is determined by the amount lost in heating of the material during extrusion and amount gained during cooling of the filament after extrusion. Material heated to higher temperatures becomes more amorphous than those at lower temperatures. Then, the use of a fan at the extruder nozzle in our setup promotes immediate cooling upon extrusion. Thus, there is limited time for order to re-form for the higher extrusion temperatures, leading to lower tensile moduli in the final filament samples.

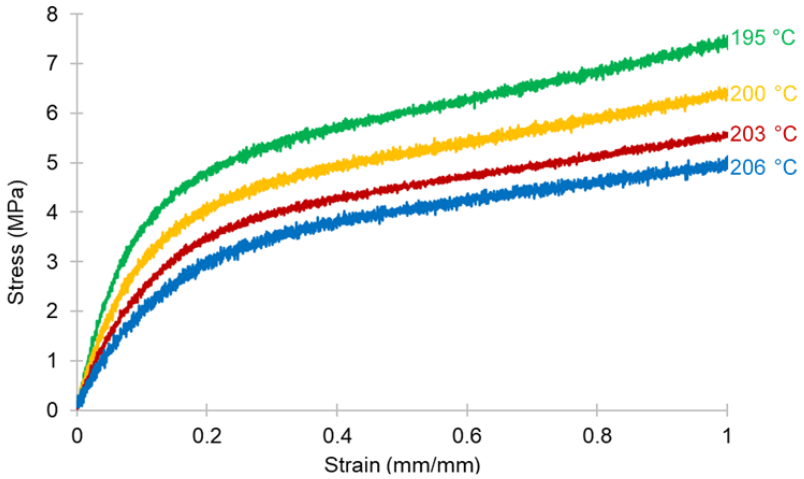

Figure 2. Elastic region of stress vs. strain curve of extruded filament from NinjaFlex pellets at varied extrusion temperatures.

3.4. Effects of magnetic particulate on mechanical properties

The processing effects on the mechanical properties of the matrix material prior to particulate loading is shown in Figure 3. Whereas all the samples have nearly the same instantaneous elastic modulus, deviations can be seen at strain of approximately 0.15. For the filaments with no particulate,

both processed sample variants (extruded pellets and solvent cast) diverge from the pre-made as purchased samples at approximately 0.15. Since all composite samples were produced using the solvent casting technique, the solvent cast data curve from Figure 3 was compared to samples with particulate loading in Figure 4 for trend analysis.

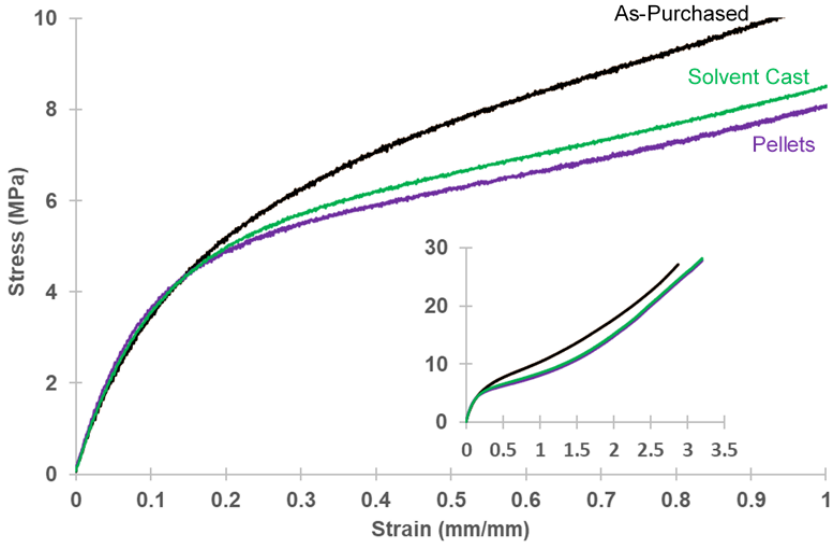

Figure 3. Effect of processing on mechanical properties of samples with no particulate loading. Full extension curves are shown in the inset.

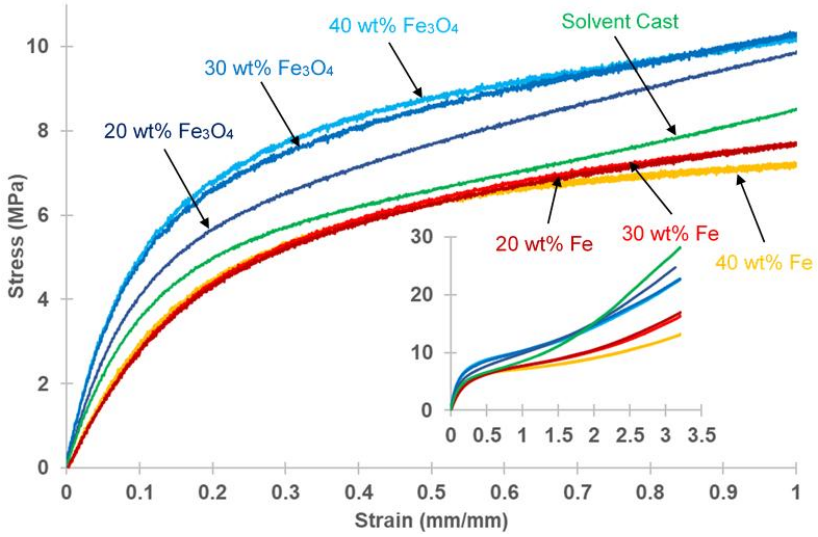

Figure 4. Impacts of particulate on mechanical properties compared to processing effects of samples with no particulate loading. Full extension curves are shown in the inset.

The impacts of the particulate loading on the mechanical properties of the filament samples are shown in Figure 4. Since most samples did not break within the limits of the apparatus used for testing tensile strength of the filaments, further testing will need to be conducted to conclude the ultimate tensile strengths of each particulate loading case. The samples with Fe particulate have a

noticebly lower stiffness than those with Fe_3O_4. As discussed below, the different responses of particulate types can be accounted for by particulate volume, size, aggregation, and interfacial adhesion [31–34].

As shown in the Einstein equation for rigid inclusions in a non-rigid matrix, volume percentage plays a key role in modifying the mechanical properties of such composites [32]. There is a smaller total volume of particulate in Fe samples when compared to Fe_3O_4 due to differences in the materials densities. Fe has a density of 7.87 g/cm^3, whereas Fe_3O_4 has a density of 5.15 g/cm^3. Refer to Table 4 for the volume percent comparisons. Thus, less of the composite sample volume is "reinforced" with Fe particulate compared to the Fe_3O_4 samples.

Table 4. Weight to volume percent comparison of particulate:TPU in Fe and Fe_3O_4 samples.

Material	Vol%
20 wt% Fe	3.64
30 wt% Fe	6.09
40 wt% Fe	9.16
20 wt% Fe_3O_4	5.46
30 wt% Fe_3O_4	9.01
40 wt% Fe_3O_4	13.35

Whereas volume percentage has the most influence on the mechanical properties, size of particulate, aggregation, and interfacial adhesion may have significant impacts as well. The decrease in size of particulate can increase the elastic modulus of elastomer matrix composites [32,34]. The theory is that at as size decreases, the surface area increases relative to total amount of material generating more interfacial bond potential.

More notably, the size of particulate plays a role in aggregation of particles. Aggregation contributes significantly to why there is such a difference between the curves of different infill type. As is demonstrated by Lee et al., the Fe_3O_4 samples have higher degrees of particulate aggregation than their Fe sample counterparts [29]. Per Pu et al., samples with aggregated particulate exhibit increased strength and stiffness relative to samples with randomly dispersed particulate [33]. These increased properties come from the interaction of strain fields within the matrix near the closely oriented particulate. This creates local regions of improved strength which in turn interact with each other and influence the universal strength and stiffness of the material.

Adhesion between the particulate interface and matrix may also play a role in altering material properties. The primary reason for a difference in adhesion between our material sample types is likely due to the surface area of the particulate. In general, interfacial adhesion increases with surface area of the particulate. It is likely, however, that the different chemistry of the infill materials may have also had an impact on the degrees of adhesion throughout mechanical testing. The degree of interfacial adhesion is an important factor when the applied stress exceeds the frictional forces [32]. Therefore, since the applied stresses do not typically exceed the frictional forces until after the instantaneous elastic regime, the impacts of interfacial adhesion in the elastic regime are likely insignificant when compared to size and aggregation of particulate. However, this factor could play a role in differences seen at higher stresses.

Some interesting observations were noted when comparing the unfilled samples to the samples with magnetic particulate. As is shown in Figure 4, the instantaneous elastic modulus of the unfilled

samples falls between that of the Fe and Fe_3O_4 samples. This is contrary to previous work demonstrating that the addition of particulate should increase the mechanical stiffness of a polymer [31,32]. This change in properties requires further investigation but is likely due to differences in the processing (e.g., different optimal extrusion temperature) and internal structure (e.g., polymer morphology) that arise due to the presence or absence of particulate during filament extrusion.

3.5. Effects of magnetic particulate on magnetic properties

The magnetic properties of the samples with magnetic particulate are shown in Figure 5. These hysteresis loops are characteristic of micron-scale Fe and Fe_3O_4 particulate and composites [35–38]. Samples with Fe particulate demonstrated clearly different properties from those with Fe_3O_4. The most noticeable difference is that Fe particulate samples have higher magnetic saturation, which is expected given that iron has a significantly greater saturation magnetization (218 emu/g) than Fe_3O_4 (92 emu/g) [39]. Additionally, as particulate percentage increases, so does saturation magnetization and susceptibility. Note that the sample size (i.e., volume) remained constant between samples to enhance measurement consistency, yet each measured sample moment was normalized by the total composite mass of each sample (particulate and TPU) to enhance measurement accuracy and precision. As a result, the nonlinear changes in the total mass-normalized composite saturation magnetizations shown in Figure 5 are due to the nonlinear increase in volume percentage of particulate relative to the diamagnetic TPU matrix material. Additionally, it should be noted that the extrusion process has a potential for contaminating filaments with magnetic particulate between extrusions, and great care should be taken to mitigate this. Due to the dominant diamagnetic behavior of our extruded unfilled samples seen in Figure 5, it is clear in this study that contamination was not a significant issue.

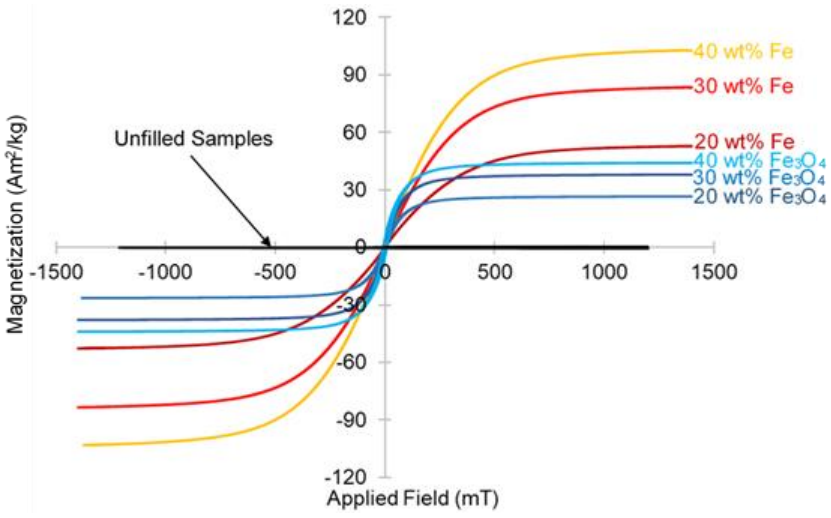

Figure 5. Impacts of particulate on magnetic properties. Magnetic hysteresis of filament samples along the long axis. Note: Total composite mass was used to calculate magnetization.

Upon closer inspection, the Fe_3O_4 samples had a larger susceptibility and demonstrated a measurable coercivity, while the Fe samples had no measurable coercivity. Figures 6 and 7 show this trend.

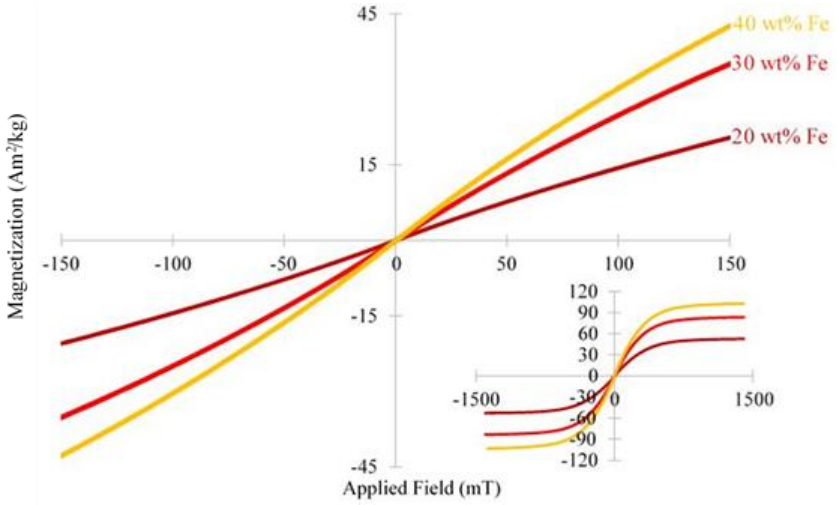

Figure 6. Coercivity of magnetic Fe filaments. Full magnetic hysteresis of Fe samples in bottom right inset.

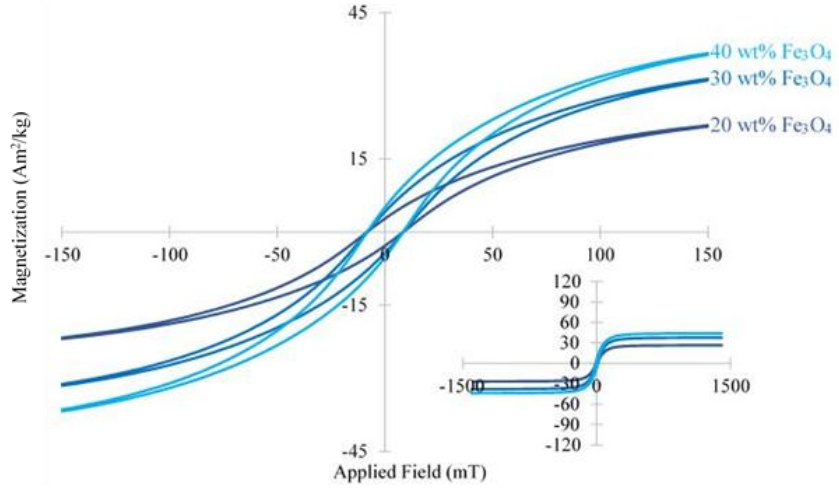

Figure 7. Coercivity of magnetic Fe_3O_4 filaments. Full magnetic hysteresis of Fe_3O_4 samples in bottom right inset.

4. Conclusion

In conclusion, the mechanical and magnetic properties of extruded filament samples were investigated as a function of various processing conditions, including magnetic particulate type, magnetic particulate percentage, extrusion temperature, and pre-extrusion preparation. The mechanical and magnetic effects of Fe and Fe_3O_4 particulate loading at different weight concentrations (20, 30, 40 wt%) were acquired utilizing a tensile testing machine and VSM. In

general, filament samples with Fe particulate had higher diametric consistency and were more compliant than those with Fe_3O_4 particulate. Additionally, samples with Fe_3O_4 had higher magnetic susceptibility and coercivity but lower saturation magnetization than those with Fe. Increasing particulate percentage increased the mechanical stiffness, magnetic saturation and susceptibility of the samples. This work demonstrates that processing a wide variety of thermoplastic magnetic elastomer filaments for FFF is feasible and opens the door to further investigations of magnetic elastomer structures created via FFF.

Acknowledgements

We would like to acknowledge the Undergraduate Research Opportunities Program at the University of St. Thomas for partial funding of this project. Part of this work was performed at the Institute for Rock Magnetism (IRM) at the University of Minnesota. The IRM is a US National Multi-user Facility supported through the Instrumentation and Facilities program of the National Science Foundation, Earth Sciences Division, and by funding from the University of Minnesota.

Conflict of interest

All authors declare no conflicts of interest in this paper.

References

1. Rafique M, Kandare E, Sprenger S (2017) Fiber-reinforced magneto-polymer matrix composites (FR–MPMCs)—A review. *J Mater Res* 32: 1020–1046.
2. Yang L, Martin L, Staiculescu D, et al. (2008) A novel flexible magnetic composite material for RFID, wearable RF and bio-monitoring applications. *2008 IEEE MTT-S International Microwave Symposium Digest* 2008: 963–966.
3. Thévenot J, Oliveira H, Sandre O, et al. (2013) Magnetic responsive polymer composite materials. *Chem Soc Rev* 42: 7099–7116.
4. Evans B, Fiser B, Prins W, et al. (2012) A highly tunable silicone-based magnetic elastomer with nanoscale homogeneity. *J Magn Magn Mater* 324: 501–507.
5. Carlson J, Jolly M (2000) MR fluid, foam and elastomer devices. *Mechatronics* 10: 555–569.
6. Schmauch M, Mishra S, Evans B, et al. (2017) Chained iron microparticles for directionally controlled actuation of soft robots. *ACS Appl Mater Inter* 9: 11895–11901.
7. Ubaidillah, Sutrisno J, Purwanto A, et al. (2015) Recent progress on magnetorheological solids: materials, fabrication, testing, and applications. *Adv Eng Mater* 17: 563–597.
8. Shamonin M, Kramarenko E (2018) Highly Responsive Magnetoactive Elastomers, In: Domracheva N, Caporali M, Rentschler E, *Novel Magnetic Nanostructures: Unique Properties and Applications*, Elsevier, 221–245.
9. Karsli N, Aytac A (2013) Tensile and thermomechanical properties of short carbon fiber reinforced polyamide 6 composites. *Compos Part B-Eng* 51: 270–275.
10. Ning F, Cong W, Qiu J, et al. (2015) Additive manufacturing of carbon fiber reinforced thermoplastic composites using fused deposition modeling. *Compos Part B-Eng* 80: 369–378.

11. Gu H, Tadakamalla S, Huang Y, et al. (2012) Polyaniline stabilized magnetite nanoparticle reinforced epoxy nanocomposites. *ACS Appl Mater Inter* 4: 5613–5624.
12. Abramchuk S, Kramarenko E, Grishin D, et al. (2007) Novel highly elastic magnetic materials for dampers and seals: Part II. Material behavior in a magnetic field. *Polym Advan Technol* 18: 513–518.
13. Stolbov O, Raikher Y, Balasoiu M (2011) Modelling of magnetodipolar striction in soft magnetic elastomers. *Soft Matter* 7: 8484–8487.
14. Guo N, Leu M (2013) Additive manufacturing: Technology, applications and research needs. *Front Mech Eng* 8: 215–243.
15. Drummer D, Cifuentes-Cuéllar S, Rietzel D (2012) Suitability of PLA/TCP for fused deposition modeling. *Rapid Prototyping J* 18: 500–507.
16. Ge C, Priyadarshini L, Cormier D, et al. (2018) A preliminary study of cushion properties of a 3D printed thermoplastic polyurethane Kelvin foam. *Packag Technol Sci* 31: 361–368.
17. Carneiro O, Silva A, Gomes R (2015) Fused deposition modeling with polypropylene. *Mater Design* 83: 768–776.
18. Ahn S, Montero M, Odell D, et al. (2002) Anisotropic material properties of fused deposition modeling ABS. *Rapid Prototyping J* 8: 248–257.
19. Tanikella N, Wittbrodt B, Pearce J (2017) Tensile strength of commercial polymer materials for fused filament fabrication 3D printing. *Addit Manuf* 15: 40–47.
20. Tibbits S (2015) Challenges and Opportunities. *3D Print Addit Manuf* 2: 151.
21. Zhong W, Li F, Zhang Z, et al. (2001) Short fiber reinforced composites for fused deposition modeling. *Mat Sci Eng A-Struct* 301: 125–130.
22. Tekinalp H, Kunc V, Velez-Garcia G, et al. (2014) Highly oriented carbon fiber–polymer composites via additive manufacturing. *Compos Sci Technol* 105: 144–150.
23. Sharma U, Concagh D, Core L, et al. (2018) The development of bioresorbable composite polymeric implants with high mechanical strength. *Nat Mater* 17: 96–102.
24. Libanori R, Erb R, Reiser A, et al. (2012) Stretchable heterogeneous composites with extreme mechanical gradients. *Nat Commun* 3: 1265.
25. Kim Y, Ribeiro L, Maillot F, et al. (2010) Bio-inspired synthesis and mechanical properties of calcite-polymer particle composites. *Adv Mater* 22: 2082–2086.
26. Nikzad M (2011) New metal/polymer composites for fused deposition modelling applications [PhD thesis]. Swinburne University of Technology, Melbourne, Australia.
27. Kim Y, Yuk H, Zhao R, et al. (2018) Printing ferromagnetic domains for untethered fast-transforming soft materials. *Nature* 558: 274–279.
28. Technical Specifications: NinjaFlex® 3D Printing Filament. Available from: https://ninjatek.fppsites.com/wp-content/uploads/2018/10/NinjaFlex-TDS.pdf.
29. Lee T, Morgenstern A, Höft T, et al. (2019) Dispersion of particulate in solvent cast magnetic thermoplastic polyurethane elastomer composites. *AIMS Mater Sci* 6: 354–362.
30. Callister W, Rethwisch D (2015) Characteristics, Applications, and Processing of Polymers, In: *Fundamentals of Materials Science and Engineering: An Integrated Approach*, 8 Eds., Wiley, 575–576.
31. Fu S, Feng X, Lauke B, et al. (2008) Effects of particle size, particle/matrix interface adhesion and particle loading on mechanical properties of particulate–polymer composites. *Compos Part B-Eng* 39: 933–961.

32. Ahmed S, Jones F (1990) A review of particulate reinforcement theories for polymer composites. *J Mater Sci* 25: 4933–4942.
33. Pu Z, Mark J, Jethmalani J, et al. (1997) Effects of dispersion and aggregation of silica in the reinforcement of poly(methyl acrylate) elastomers. *Chem Mater* 9: 2442–2447.
34. Drozdov A, Dorfmann A (2001) The stress–strain response and ultimate strength of filled elastomers. *Comp Mater Sci* 21: 395–417.
35. Abramchuk S, Kramarenko E, Stepanov G, et al. (2007) Novel highly elastic magnetic materials for dampers and seals : Part I. Preparation and characterization of the elastic materials. *Polym Advan Technol* 18: 883–890.
36. Boczkowska A, Awietjan SF, Wejrzanowski T, et al. (2009) Image analysis of the microstructure of magnetorheological elastomers. *J Mater Sci* 44: 3135–3140.
37. Li J, Zhang M, Wang L, et al. (2011) Design and fabrication of microfluidic mixer from carbonyl iron–PDMS composite membrane. *Microfluid Nanofluid* 10: 919–925.
38. Masłowski M, Strąkowska A, Strzelec K (2017) Magnetic (ethylene–octene) elastomer composites obtained by extrusion. *Polym Eng Sci* 57: 520–527.
39. Cullity B (1972) Ferrimagnetism, In: *Introduction to Magnetic Materials*, Menio Park: Addison-Wesley Publishing Company, 190.

AIMS Press